
Proceedings Paper:
Iyasara, A.C., Schmidt, W.L., Boston, R. et al. (2 more authors) (2017) La and Sm Co-doped SrTiO3-delta Thermoelectric Ceramics. In: Materials Today: Proceedings. European Materials Research Spring Meeting, Symposium H, 22-26 May 2017, Strasbourg, France. Elsevier , pp. 12360-12367.

https://doi.org/10.1016/j.matpr.2017.10.004

Available online at www.sciencedirect.com

ScienceDirect

Materials Today: Proceedings 00 (2017) 0000–0000

www.materialstoday.com/proceedings

EMRSH_2017

La and Sm Co-doped $SrTiO_{3-\delta}$ Thermoelectric Ceramics

Adindu C. Iyasara[a], Whitney L. Schmidt[a], Rebecca Boston[a], Derek C. Sinclair[a], and Ian M. Reaney *[a]

[a]Functional Materials and Devices Group, Department of Materials Science and Engineering, University of Sheffield, Sheffield, S1 3JD, UK.

Abstract

The thermoelectric properties of $Sr_{1-x}La_{x/2}Sm_{x/2}TiO_{3-\delta}$ ($0.05 \leq x \leq 0.30$) ceramics have been investigated with compositions batched, synthesised by solid state reaction and sintered in 5% H_2/N_2 at 1500 °C for 6 hrs. All X-ray diffraction patterns were fully indexed according to a cubic perovskite phase. Scanning electron microscopy revealed homogeneous grain structure in the ceramics and confirmed relative density ≥ 89 %. The electrical conductivity (σ) of $x \leq 0.15$ displayed metallic behaviour with $\sigma <$ 1000 S/cm, whereas $x \geq 0.20$ were semiconducting with $\sigma <$ 250 S/cm. The Seebeck coefficient of all compositions was negative indicating n-type behaviour. Within this series, x = 0.20 displayed the lowest thermal conductivity of ~ 3 W/m.K (at 973 K), x = 0.10 displayed the highest power factor of 1400 $\mu W/K^2.m$ (at 573 K) and overall x = 0.15 had the highest dimensionless figure of merit (ZT) of 0.24 (at 875 K).

Selection and/or Peer-review under responsibility of EMRS Spring Meeting, symposium H.

Keywords: Thermoelectrics; Solid state reaction; Seebeck coefficient; Power factor; Figure of merit.

1. Introduction

Non-renewable energy based on fossil fuels currently remain the most widely used source of electricity generation. The high cost of these fuels and their attendant environmental pollution, emissions of greenhouse gases have resulted in research towards the development of alternative energy sources and means to recover wasted energy from existing sources [1,2]. Amongst these promising energy solutions, thermoelectric (TE) materials have received significant attention as a way of converting waste heat energy back into a useable form. TE materials have the capacity to generate

* Corresponding author. Tel.: +44 (0)114 222 5471
E-mail address: i.m.reaney@sheffield.ac.uk

Selection and/or Peer-review under responsibility of EMRS Spring Meeting, symposium H.

electrical power using a temperature difference (power generation) or to convert electrical power into a temperature difference (which can be used for applications such as solid state refrigeration) [3].

The performance of TE materials is evaluated using the dimensionless figure of merit, ZT, defined by:

$$\boldsymbol{ZT = \frac{S^2 \sigma T}{k}} \quad (1)$$

where S is the Seebeck coefficient, σ is the electrical conductivity, T is the absolute temperature at which the properties are measured, and k is the total thermal conductivity. From Equation 1, the power factor (PF), PF = $S^2\sigma$ can be determined and is a measure of the electrical power anticipated from a TE device [4]. The higher the value of ZT, the higher the efficiency of the TE material. It is clear from equation 1 that high values of ZT therefore require a high PF and a low k [5].

Non-oxide intermetallic compounds such as Bi_2Te_3/Se_3, Sb_2Te_3, PbTe/Se, SiGe and their corresponding alloys are the most extensively studied TE materials [6] mainly because they possess small phonon group velocity and low k, desirable for optimized ZT. The broad application of these materials is limited, however, due to toxicity, scarcity, cost, and limited operational temperature range [7]. There is evidence, however, that transition-metal oxide thermoelectric materials are viable alternatives that may, given improvements in ZT, surmount the challenges associated with non-oxides [8-11].

Reduced rare earth (RE) doped $SrTiO_3$ ceramics have recently been shown to have promising TE properties [12,13]. $SrTiO_3$ as an end-member material has been widely studied in terms of the effect of different dopants doping mechanisms, and processing conditions [14]. The most common RE doping mechanism is based on A-site donor doping via an electronic mechanism, i.e. $RE^{3+} + e^- \rightarrow Sr^{2+}$ (general formula $Sr_{1-x}RE_xTiO_3$) in attempts to increase σ. Despite reported high S, high σ, and large PF, ZT remains low due to high k when compared with non-oxide TE materials [7].

The aim of this research is to study the structure-property relationships of co-doped RE $SrTiO_{3-\delta}$ ceramics based on the electronic doping sintered in 5% H_2/ N_2 gas mixtures. The purpose of co-doping instead of single doping is an attempt to enhance the phonon scattering and therefore reduce k without significantly affecting the PF. To do this, we select La as the largest RE ion and Sm as an intermediate sized RE ion to give a significant variation in the ionic radius and mass of these A-site doping ions compared to Sr.

2. Experimental procedure

2.1 Ceramic processing

Compositions of $Sr_{1-x}La_{x/2}Sm_{x/2}TiO_{3-\delta}$ ($0.05 \leq x \leq 0.30$) were prepared by a solid state reaction method from $SrCO_3$ (99.90 %, Sigma-Aldrich, UK), La_2O_3 (99.99 %, Sigma-Aldrich, UK), Sm_2O_3 (99.90 %, Stanford Materials Corporation, USA) and TiO_2 (99.90 %, Sigma-Aldrich, UK) as starting materials. These starting reagents were dried and stoichiometric quantities mixed by ball milling in isopropanol using 10 mm yttria-stabilised zirconia milling media for 24 hours. The mixed powders were dried at ~ 90 °C, sieved through a 250 μm mesh and calcined at 1573 K in air for 6 hours using an alumina crucible [15].

The calcined powders were mixed and ground with 5 wt.% poly vinyl alcohol binder and then pressed into 20 mm diameter pellets using a uniaxial steel press using 1 ton of applied load for ~ 1 minute. The pellets were pre-sintered

in air at 873 K for 1 hour to burn-off the binder and then sintered in 5 % H_2/N_2 flowing gas at 1773 K for 6 hours. Finally, the sintered ceramics were wet polished to remove surface impurities and to produce smooth (and flat) surface samples. The experimental density of the samples was determined by applying Archimedes principle using an electronic digital density balance (Mettler-Toledo AG balance).

2.2 Structural and microstructural investigation

The phase assemblage and crystal structures of crushed sintered pellets were characterised by powder X-ray diffraction (XRD) with Cu K_α radiation (λ = 1.5406 Å) at room temperature using a Siemens D 5000 diffractometer. Scans were conducted over a scan range from 20 to 80 ^{o} 2θ using a step size of 0.01^o and a scan rate of 1 ^{o}/min. The collected data were analysed using Diffrac.Suite Eva.

Samples for microstructural examination were prepared by grinding and polishing on a diamond polishing wheel. The polished samples were thermally etched at 90 % of the sintering temperature in 5 % H_2/N_2 gas for 30 minutes. After carbon coating of the samples, the microstructures were studied using a Philips XL 30 S FEG scanning electron microscope.

2.3 Thermoelectric properties

The Seebeck coefficient and electrical conductivity of disc samples with diameters ≤ 20 mm were measured simultaneously in an argon atmosphere over a temperature range of 573-973 K using a Netzsch SBA 458 Nemesis Seebeck and electrical conductivity analyser. The thermal properties (thermal diffusivity, λ; specific heat capacity, C_p and thermal conductivity, k) were measured using a high-speed Xenon discharge pulse source on 10 x 10 mm^2 square samples using a Anter Flashline TM 3000 thermal properties analyser.

3. Results and discussion

3.1 Crystal structure

The XRD patterns of the crushed ceramics sintered in 5% H_2/N_2 at 1773 K for 6 hours are shown in Figure 1. All major peaks could be indexed on a simple cubic perovskite cell (space group Pm-3m), however x =0.05, 0.2 and 0.3 exhibited weak intensity peaks (<1% relative intensity) that corresponded to TiO_2. The absence of a trend for the appearance of second phase as a function of x suggests that the residual TiO_2 is most likely due to unreacted raw material. The lattice parameters, cell volumes and theoretical density were determined by manual calculation using the XRD data and the results are shown in Table 1.

The lattice parameter of the ceramics decreases progressively with increasing doping level, $0.05 \leq x \leq 0.20$ and then levels off at a value of ~ 3.903 Å. The decrease is attributed to the smaller ionic radii of La^{3+} (1.36 Å in co-ordination number (CN) 12) and Sm^{3+} (1.24 Å in CN 12) in the substitution for large Sr^{2+} ions (1.44 Å in CN 12) [5, 16-18]. Kovalevsky et al. have shown a tetragonal phase for Sm^{3+} doping and 3.9096(3) Å for $Sr_{0.9}La_{0.1}TiO_{3\pm\delta}$ [13]. Our data suggests that the co-doping inhibits the apparent distortion to tetragonal but without further diffraction data (electron, neutron) it is difficult to determine whether co-doping has suppressed the distortion or reduced its scale length to below the detection of the X-ray diffractometer. However, we conclude that La and Sm had become incorporated onto the A-site of the perovskite lattice in accordance with the batched formula. Further crystallographic study would provide more insight on the lattice distortions and incorporation of the co-doped elements, and provide clarification on the solid solution limit.

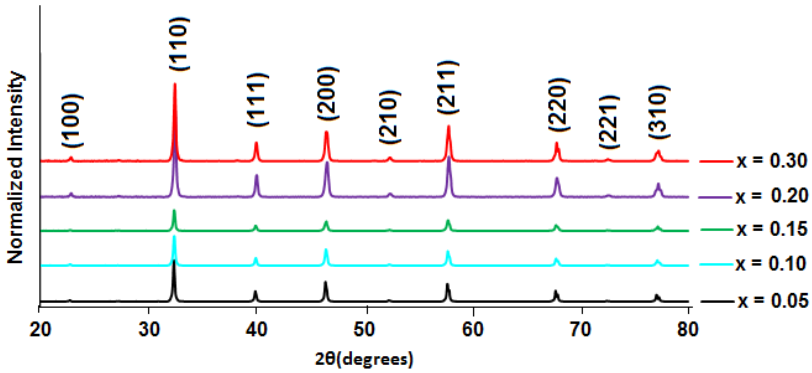

Figure 1. XRD patterns of $Sr_{1-x}La_{x/2}Sm_{x/2}TiO_{3-\delta}$ ($0.05 \leq x \leq 0.30$) ceramics sintered in 5% H_2/N_2 at 1773 K for 6 hours.

Table 1. Lattice parameter (a), cell volume (a^3), theoretical, (ρ_{th}), experimental (ρ_e) and relative density (ρ_r) of $Sr_{1-x}La_{x/2}Sm_{x/2}TiO_{3-\delta}$ ceramics sintered in 5 % H_2/N_2 at 1773 K for 6 hours.

x	a (Å)	a^3 (Å^3)	ρ_{th} (g/cm^3)	ρ_e (g/cm^3)	ρ_r (%)
0.05	3.910(6)	59.802	5.17	5.05	97.6
0.10	3.907(9)	59.682	5.26	5.14	97.7
0.15	3.907(7)	59.673	5.34	5.15	96.4
0.20	3.903(2)	59.465	5.44	4.94	90.8
0.30	3.904(9)	59.582	5.59	5.00	89.4

3.2 Microstructure

After sintering all samples had a relative density of ≥ 89 % (Table 1). SEM images of the thermally etched, carbon coated surfaces for $Sr_{1-x}La_{x/2}Sm_{x/2}TiO_{3-\delta}$ ceramics are shown in Figure 2. The SEM images of $0.05 \leq x \leq 0.15$ ceramics revealed homogeneous and dense structures consistent with their high relative density of ~ 97 %. The images of x = 0.20 and 0.30 ceramics showed evidence of porosity consistent with a lower relative density of ~ 90 %. The lower density of $x \geq 0.2$ most likely relates to the more refractory nature of La and Sm oxide in comparison to $SrTiO_3$ and suggests that further optimisation of sintering conditions is required to achieve higher densities. The impact of porosity in these compositions is unclear. Some authors suggest that the presence of pores create discontinuities in the lattice which act as scattering centres, impede carrier mobility and enhance phonon scattering [19]. In consequence, σ is decreased due to the restricted carrier mobility [19,20], while k is decreased by additional phonon scattering by the pores [19]. These pores in the SEM images may therefore contribute to the very low σ and low k values observed in the $x \geq 0.20$ ceramics.

3.3 Thermoelectric properties

The temperature dependence of the thermoelectric properties (σ, S, k, PF and ZT) of $Sr_{1-x}La_{x/2}Sm_{x/2}TiO_{3-\delta}$ ($0.05 \leq x \leq 0.30$) ceramics sintered in 5% H_2/N_2 at 1773 K for 6 hours are shown in Figure 3. Figure 3a indicates that σ for $x \leq 0.15$ decreases with increasing temperature, showing typical metallic-type behaviour. At high dopant levels ($x \geq 0.20$), a switch from metallic to semiconducting behaviour was observed. The switch from metallic to semiconducting behaviour is currently the subject of further investigation. The highest electrical conductivity recorded was 942 S/cm at 573K for x = 0.15. Seebeck coefficients of all the ceramics are negative (Figure 3b), revealing that electrons are the dominant carriers. S increases linearly with increasing temperature, showing metallic behaviour, but decreases with increasing doping level. For example, $|S| \sim 263$ μV/K for x = 0.05 at 973 K and decreases to ~ 119 μV/K for x = 0.30

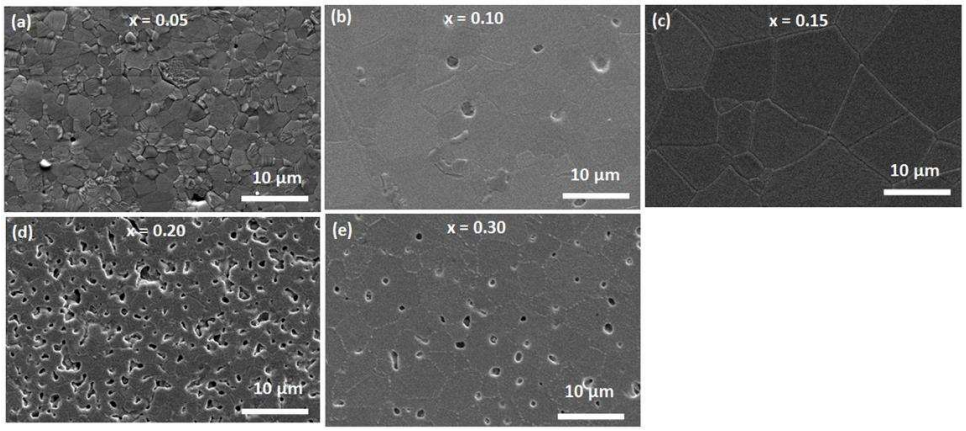

Figure 2. SEM images of the surfaces of $Sr_{1-x}La_{x/2}Sm_{x/2}TiO_{3-\delta}$ ($0.05 \leq x \leq 0.30$) ceramics sintered in 5% H_2/N_2 at 1773 K for 6 hours and thermal etched at 1623 K for 30 min.

at 973 K. The power factor, $S^2\sigma$, can then be calculated. The power factors for the different compositions are presented in Figure 3c. As the temperature increases, PF for $0.05 \leq x \leq 0.15$ ceramics decreases progressively in the entire measured temperature range. For $x \geq 0.20$, the PF increases with increasing temperature over the measured range but with very low values. x = 0.10 exhibits the highest PF of ~1400 $\mu W/K^2.m$ at 573 K. The interplay of Seebeck coefficient and conductivity in reduced oxide compositions to give PF values is complex. The O stoichiometry is most likely inhomogeneous with bulk having higher oxygen concentration than the grain boundary regions. The resulting inhomogeneous electrical microstructure may result in differing Seebeck coefficients and conductivities as a function distance within the sample, with the macroscopic properties representing average behaviour. Total thermal conductivity, k, Figure 3d, decreases with increasing temperature within the measured temperature range, suggesting that heat transfer is controlled in the samples by phonon scattering [22,23]. The increase in the phonon scattering is attributed to the size and mass difference between the A-site dopants (La and Sm) and host (Sr) species. The lowest value of k is observed for x = 0.20 ceramic with a value of 3.0 W/m.K at 973 K. However, we note that the increase in porosity will also play a role in reducing thermal conductivity.

Overall, x = 0.15 possesses the highest ZT value (0.24) at 875 K due to the relatively high PF and low k as shown in Figure 3e. There are a wide range of values reported for RE-doped $SrTiO_3$, the majority of which relate to the same electronic compensation mechanism discussed in this contribution [13,18, 24]. These reported ZT values for reduced bulk polycrystalline strontium titanates include 0.22 at 573 K for $Sr_{0.9}Dy_{0.1}TiO_3$ and 0.28 at 873 K for $Sr_{0.9}Nd_{0.1}TiO_3$ [13, 18, 24], 0.22 at 800 K for $Sr_{0.92}La_{0.08}TiO_3$ and 0.17 at 1045 K for $SrTi_{0.90}Ta_{0.1}TiO_3$ [18], 0.24 at 1073 K for $Sr_{0.9}Sm_{0.1}TiO_3$ and 0.31 at 1023 K for $Sr_{0.8}La_{0.18}Yb_{0.02}TiO_3$ [13], and 0.36 at 1045 K for $La_{0.1}Sr_{0.83}Dy_{0.07}TiO_3$ [13, 24]. Perhaps the most significant data however, was presented by Lu et al. [18] who studied La-doped $SrTiO_3$ but batched their ceramics in accordance with an ionic (A-site vacancy) compensation mechanism, $Sr_{1-3x}La_{2x}TiO_{3}$.. Lu et al. [18] concluded that A-site cation vacancies played in significant role in enabling the ingress and egress of O which was pivotal in influencing the concentration and distribution of charge carriers according to equation 2,

$$\boldsymbol{O_o^x \rightarrow \ddot{V}_o + 2e' + \frac{1}{2}O_2(g)} \qquad (2)$$

resulting in larger PFs than reported here. The net result overall was a higher ZT (0.41) at 973 K.

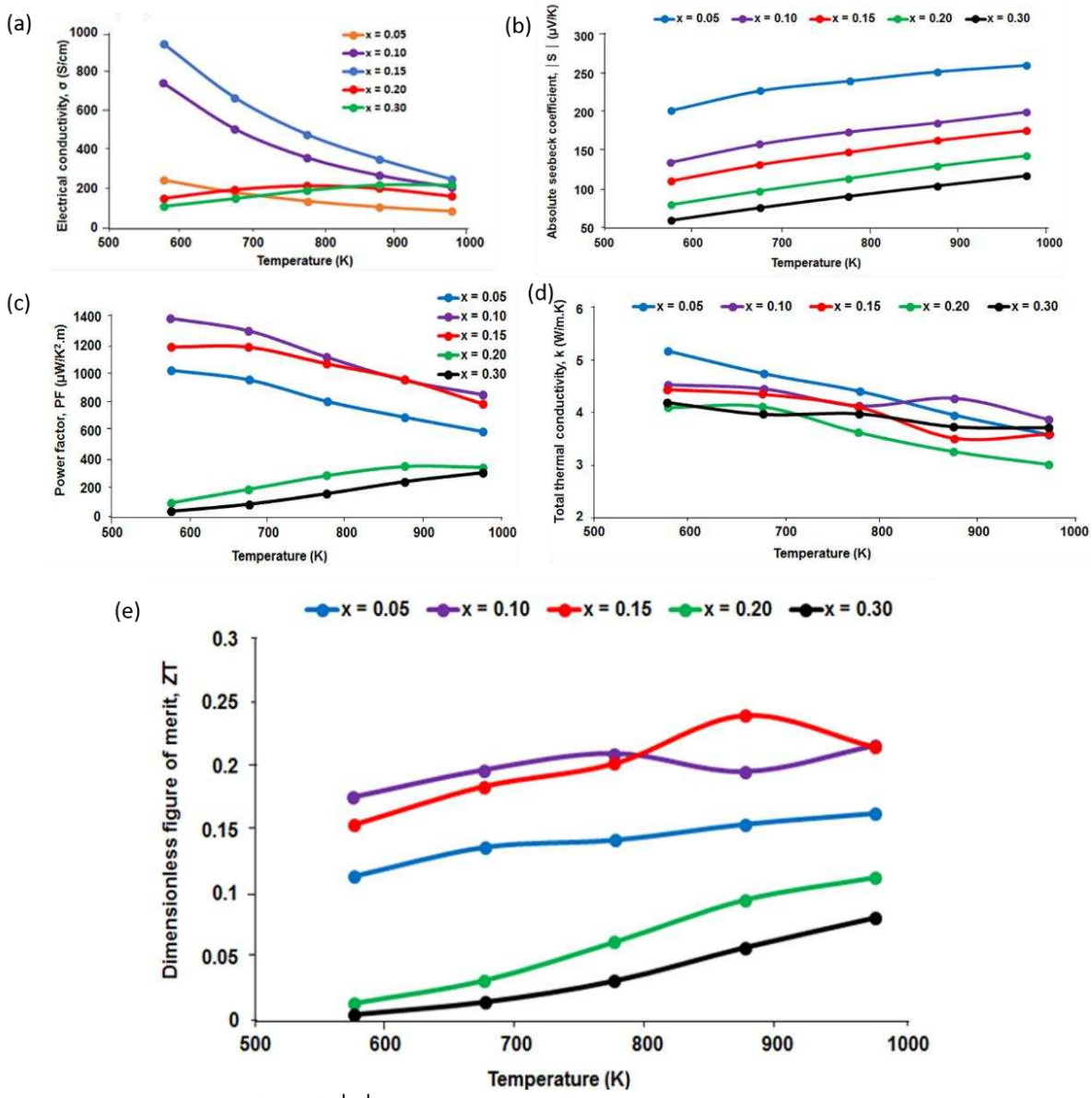

Figure 3. Temperature dependence of (a) σ (b) $|S|$ (c) PF (d) k and (e) ZT for $Sr_{1-x}La_{x/2}Sm_{x/2}TiO_{3-\delta}$ ($0.05 \leq x \leq 0.30$) ceramics sintered in 5% H_2/N_2 at 1773 K for 6 hours.

Sm and La were chosen as co-dopants in this study to test the hypothesis that a range of ions with mass and ionic radius dissimilar to Sr on the A-site would enhance phonon scattering and decrease k whilst simultaneously acting as a donor dopant, potentially increasing the carrier concentration. Evidence is presented that La and Sm co-doping enhances ZT in part through a reduction in k (3.0 W/m.K, x = 0.2). However, as the RE dopant concentration increases, the electrical conductivity decreases with a commensurate decrease in the PF. Compositions with x = 0.15, with the highest ZT, reflect an optimum compromise between reducing k and maintaining metallic behaviour with high σ. The switch from metallic to semiconducting behaviour as a function of x is currently under investigation but may relate to structural phase transitions involving rotations of the O-octahedra which are known to occur in RE-doped $SrTiO_3$ [18].

4. Conclusions

Here we have presented a novel electronically co-doped $SrTiO_3$ material with ZT of 0.24 at 875 K. Co-doping with La and Sm suppresses or decreases the scale length of a previously observed tetragonal distortion associated with Sm as a single dopant, a point to be investigated further. Co-doping had minimal effect on k leading to the conclusion that optimising ZT by this method is of limited value. In light of the work reported here and by Lu et al. [18] we suggest that batched stoichiometries which favour the formation of A-site vacancies are more important to optimising ZT.

Acknowledgements

ACI acknowledges financial support from Tertiary Education Trust Fund (TETFUND), Nigeria and Akanu Ibiam Federal Polytechnic, Unwana, Nigeria. RB acknowledges support from Lloyd's Register Foundation and Royal Academy of Engineering under the Research Fellowships scheme. All authors acknowledge the EPSRC grant EP/L017563/1 for funding.

References

[1] U.S. Energy Information Administration, International Energy Outlook DOE/EIA-0484, (2013).
[2] T. Jarman, E. E. Khalil, E. Khalaf, Open J. of Energy Efficiency, 2 (2013), 143-153.
[3] S. Lin, J. Selig, J. Alloy Compd., 31 (2010), 15-24.
[4] S. Lee, J. A. Bock, S. Trolier-McKinstry, C. A. Randall, J. Eur. Ceram. Soc., 32 (2012), 3971-3988.
[5] H. Wang, C. Wang, Ceram. Int., 39, (2013), 941-946.
[6] Z. Tian, S. Lee, G. Chen, (2014), arXiv:1401.0749.
[7] J. Liu, C. L. Wang, Y. Li, W. B. Su, Y. H. Zhu, J. C. Li, L. M. Mei, J. Appl. Phys., 114 (2013), 223714.
[8] K. Koumoto, I. Terasaki, R. Funahashi, MRS Bull., 31 (2006), 206-210.
[9] I. Terasaki, J. Appl. Phys., 110 (2011), 053705.
[10] J. F. Li, W. S Liu, L. D. Zhao, M. Zhou, Asia Mater., 2 (2010), 152–158.
[11] R. R. Sun, X. Y. Qin, L. L. Li, D. Li, N. N. Wang, J. Zhang, Q. Q. Wang, J. Appl. Phys., 112 (2012), 124904.
[12] I. M Backhaus-Ricoult, J. Rustad, L. Moore, C. Smith, J. Brown, Appl. Phys. A, 116 (2014), 433-470.
[13] A. V. Kovalevsky, A. A. Yaremchenko, S. Populoh, P. Thiel, D. P. Fagg, A. Weidenkaff, J. R. Frade, Phys. Chem. Chem. Phys., 16 (2014), 26946-26954.
[14] D. Srivastava, C. Norman, F. Azough, M. C. Schäfer, E. Guilmeau, D. Kapaptsoglou, Q. M. Ramasse, G. Nicotra, R. Freer, Phys. Chem. Chem. Phys, 18 (2016), 26475-26486.
[15] R. Boston, W. L. Schmidt, G. D. Lewin, A. C. Iyasara, L. Lu, H. Zhang, D. C. Sinclair, I. M. Reaney, Chem. Mater. 29 (2016), 265-280.
[16] H. C. Wang, C. L. Wang, W. B. Su, J. Liu, Y. Sun, H. Peng, L. M Mei, J. Am. Ceram. Soc., 94 (2011), 838-842.
[17] H. C. Wang, C. L. Wang, W. B. Su, J. Liu, Y. Zhao, H. Peng, J. L. Zhang, M. L. Zhao, J. C. Li, N. Yin, L. M. Mei, MRS Bull., 45, (2010), 809-812.
[18] Z. Lu, H. Zhang, W. Lei, D. C. Sinclair, I. M. Reaney, Chem. Mater., 28 (2016), 925-935.
[19] C-S Park, M-H Hong, H. H Cho, H-H Park, Appl. Surf. Sci., 409 (2017), 17 – 21.
[20] M-H Hong, Ch-S Park, S. Shin, H. H Cho, W-S Seo, Y.S Lim, J. K Lee, H-H Park, J. Nanomater., 2013 (2013), 172504.
[21] H. C. Wang, C. L. Wang, W. B. Su, J. Liu, Y. Sun, H. Peng, L. M. Mei, J Am. Ceram. Soc., 94 (2011), 838-842.
[22] G. H Zheng, Z. X Dai, Y. Q Dong, F. L Zan, D. Zou, Y Q Ma and G. Li, Mat. Res. Inno., 16 (2012), 438 – 441.
[23] C. Yu, M. L Scullin, M. Huijben, R. Ramesh and A. Majumdar, Appl. Phys. Lett, 92 (2008), 191911- 191913.
[24] A. V. Kovalevsky, A. A. Yaremchenko, S. Populoh, A. Weidenkaff, J. R. Frade, J. Phys. Chem. C, 118 (2014), 4596-4606.